

SUPPLEMENTARY MATERIAL

Doxorubicin delivery performance of superparamagnetic carbon multi-core shell nanoparticles: pH dependence, stability and kinetic insight

Adriano Santos Silva,^a Jose Luis Diaz de Tuesta,^{*b} Thais Sayuri Berberich,^{a,b} Simone Delezuk Inglez,^b Ana Raquel Bertão,^c Ihsan Çaha,^c Francis Leonard Deepak,^c Manuel Bañobre-López,^c and Helder Teixeira Gomes^a

^a Centro de Investigação de Montanha (CIMO), Instituto Politécnico de Bragança, Campus Santa Apolónia, 5300-253, Bragança, Portugal.

^b Universidade Tecnológica Federal do Paraná, Campus Ponta Grossa, 84017-220, Ponta Grossa, Paraná, Brazil.

^c Advanced (Magnetic) Theranostic Nanostructures Lab, International Iberian Nanotechnology Laboratory, Av. Mestre Jose Veiga s/n, 4715-330 Braga, Portugal.

* corresponding author: jl.diazdetuesta@ipb.pt

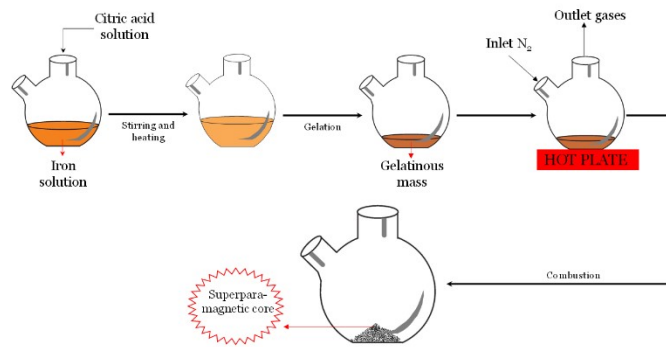


Figure S1. Synthesis of the superparamagnetic core by SCS.

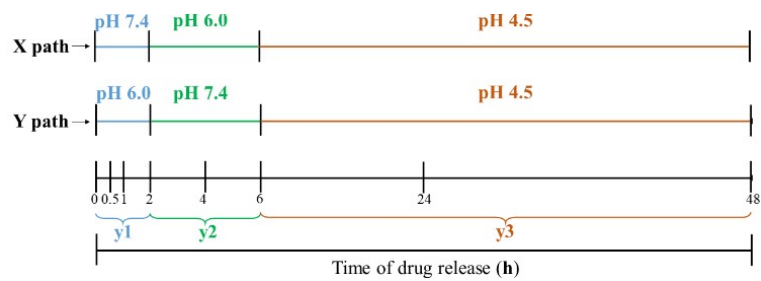


Figure S2. Path test for drug delivery (distances between are illustrative).

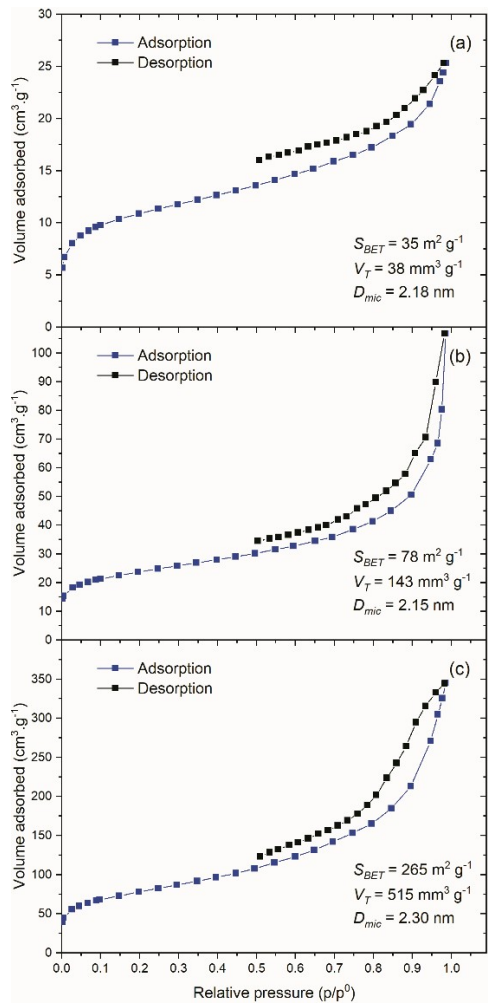


Figure S3. N₂ adsorption isotherms at 77 K for a) bare magnetite, b) Fe₃O₄/S@C, and c) Fe₃O₄@C.

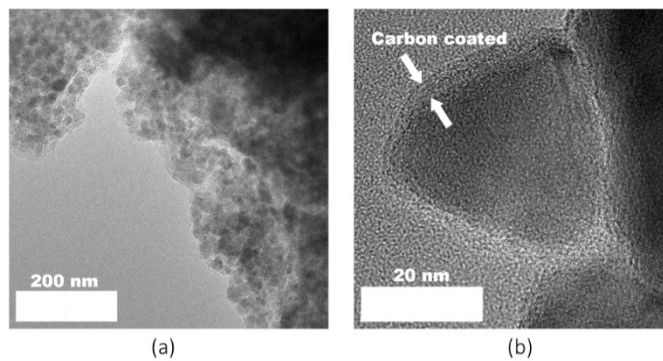


Figure S4. TEM images of a) magnetite and b) Fe₃O₄@C_PF127.

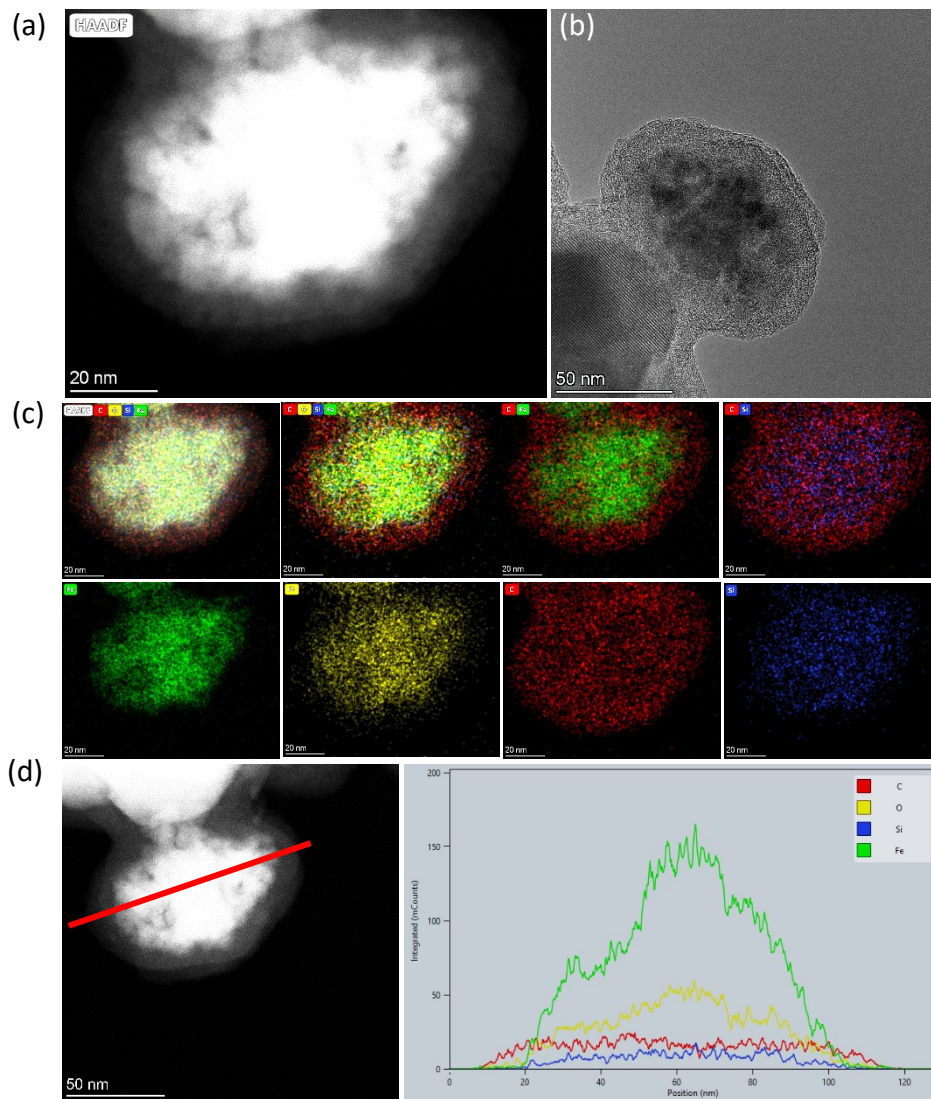


Figure S5. Before etching ($\text{Fe}_3\text{O}_4/\text{SiO}_2@\text{C}$). a) HAADF-STEM image of a core-shell magnetic aggregate. b) TEM image highlighting the multi-core composition of the core-shell nanostructures and the crystalline structure of the magnetite nanoparticles. c) Energy-Dispersive X-ray Spectroscopy (EDX) elemental mapping of sample $\text{Fe}_3\text{O}_4/\text{SiO}_2@\text{C}$ showing the spatial distribution of C, Fe, O and Si elements in the structure. d) STEM-EDX line scan analysis along one single core-shell nanostructure by measuring the intensity of the characteristic spectral lines of C, Fe, O and Si elements.

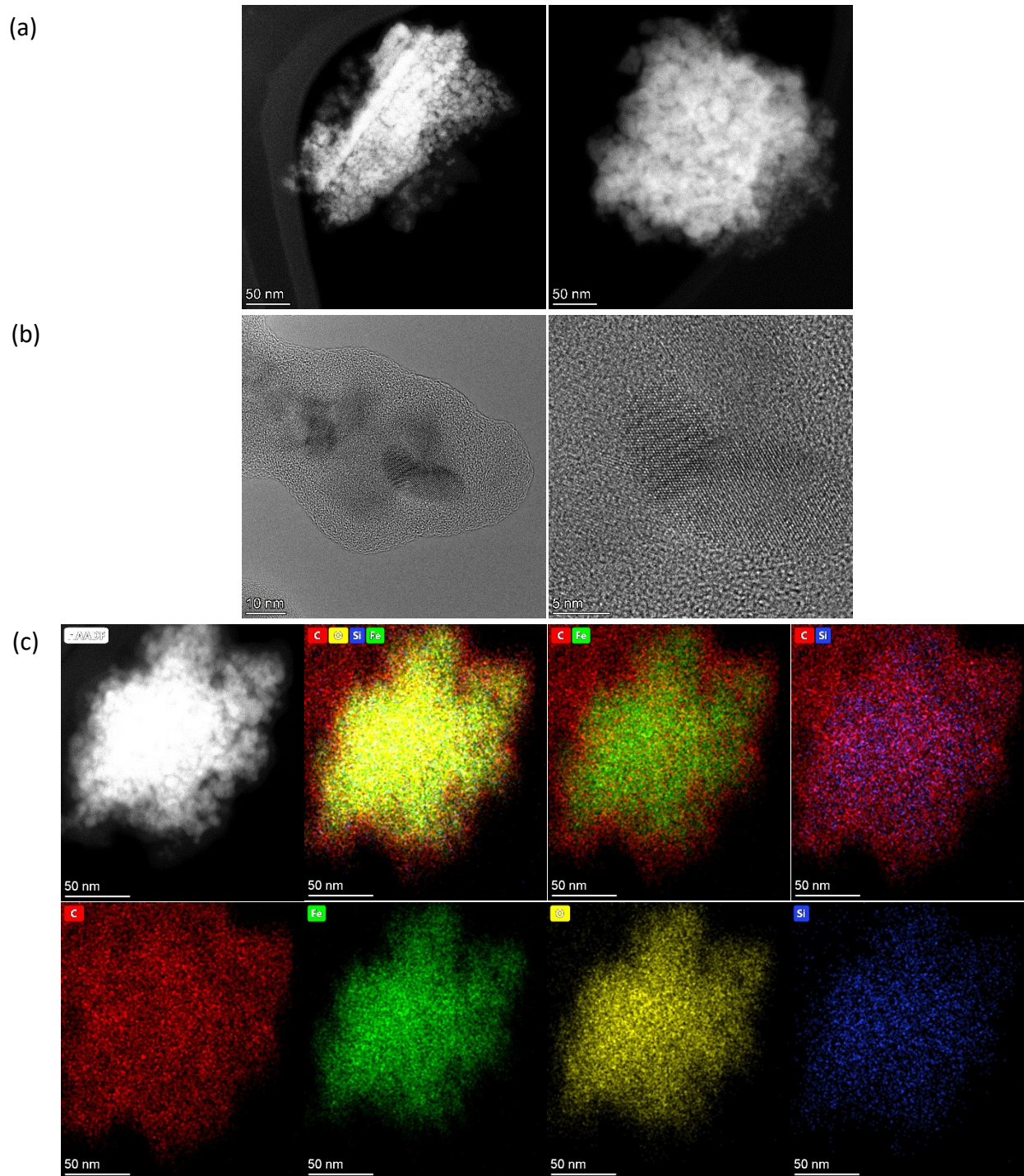


Figure S6. After Si etching ($\text{Fe}_3\text{O}_4@\text{C}$). (a) HAADF-STEM image of a core-shell magnetic aggregate. (b) TEM image highlighting the multi-core composition of the core-shell nanostructures and the crystalline structure of the magnetite nanoparticles. (c) Energy-Dispersive X-ray Spectroscopy (EDX) elemental mapping of sample $\text{Fe}_3\text{O}_4@\text{C}$ showing the spatial distribution of C, Fe, O and Si elements in the structure.

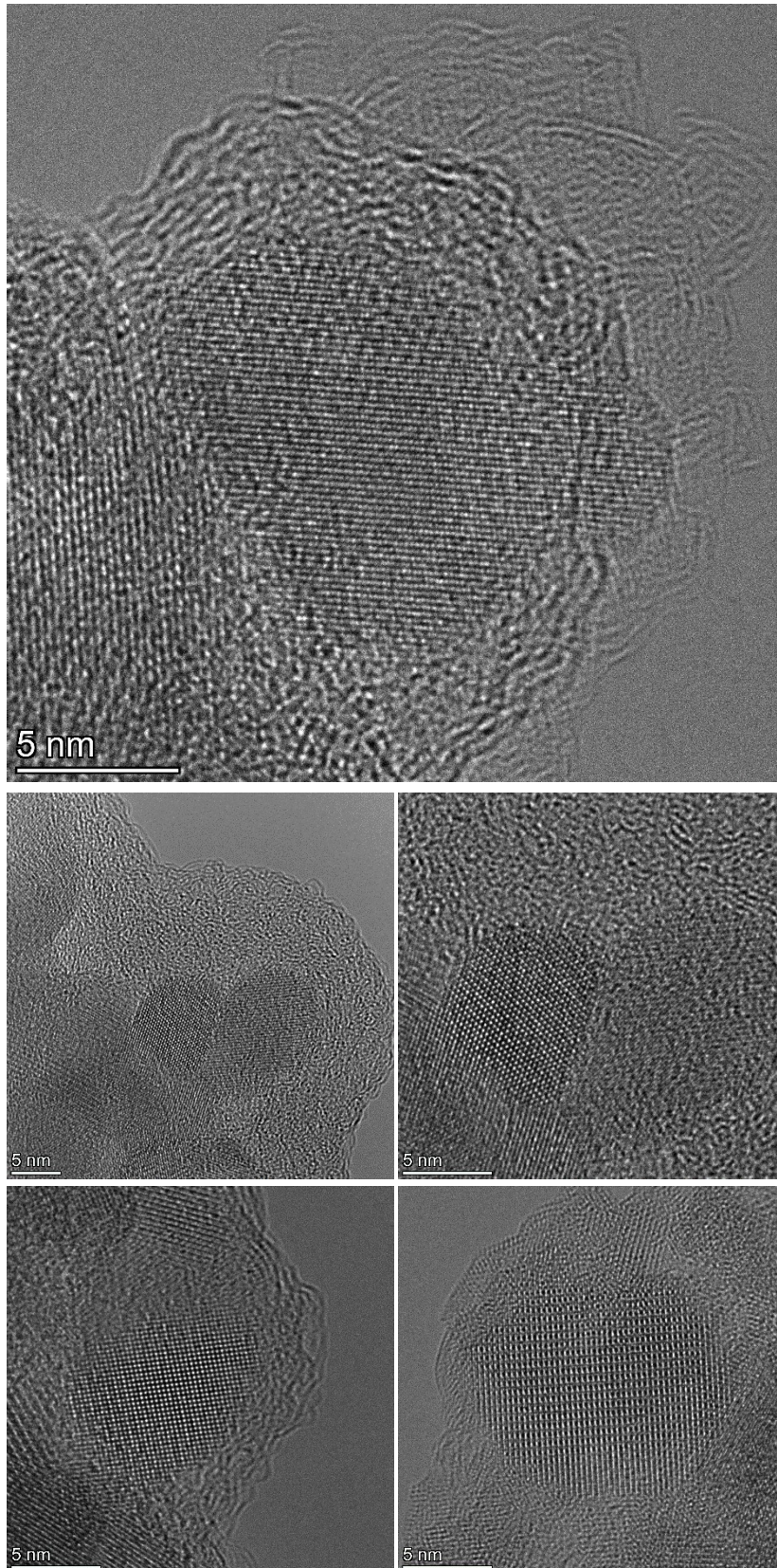


Figure S7. After Si etching, TEM images of different core-shell magnetic aggregates where a partial crystallization of the C coating can be observed.

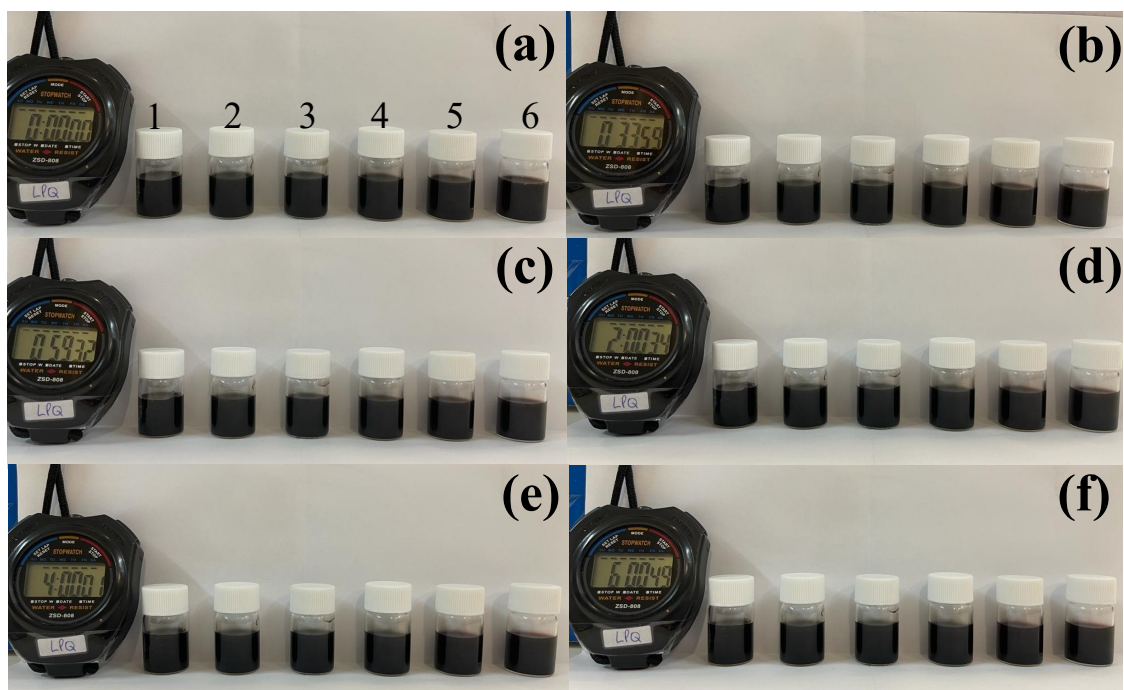


Figure S8. Stability of the $\text{Fe}_3\text{O}_4@\text{C_PF127}$ suspension in 1) distilled water, PBS 2) 4.5, 3) 6.0, 4) 7.4, 5) DMEM and 6) DMEM1 for a) 0, b) 0.5 c) 1, d) 2, e) 4 and f) 6 h. NPs concentration in all flasks was 1 mg mL^{-1} .

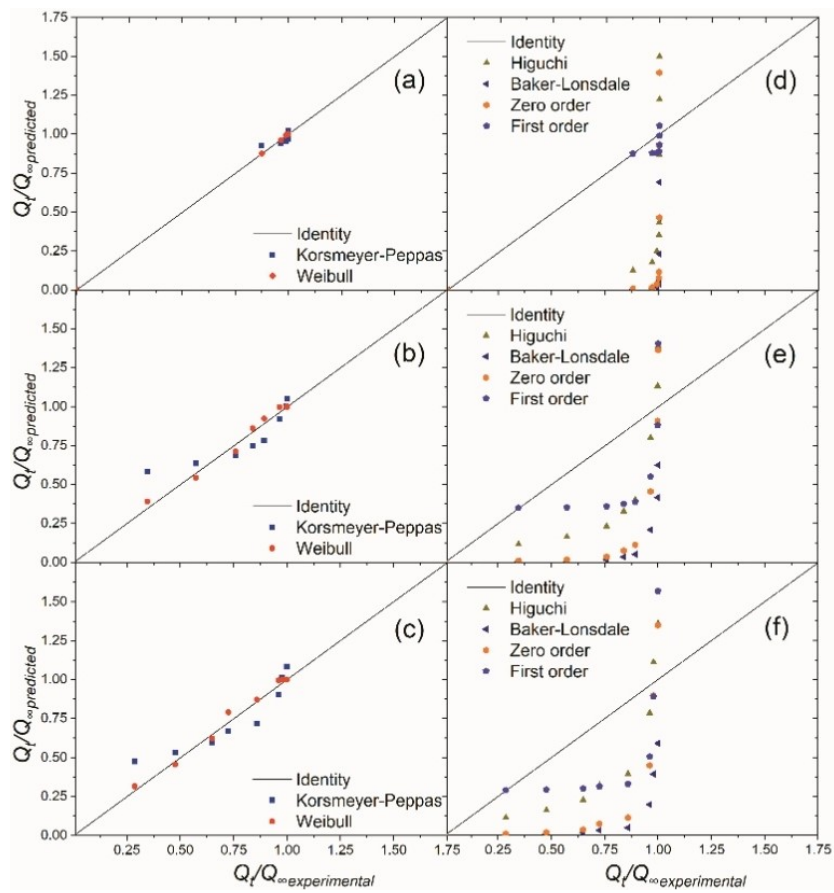


Figure S9. Parity plots for Korsmeyer-Peppas and Weibull predictions for drug release in pH a) 4.5, b) 6.0, and c) 7.4; and other models in pH d) 4.5, e) 6.0, and f) 7.4.

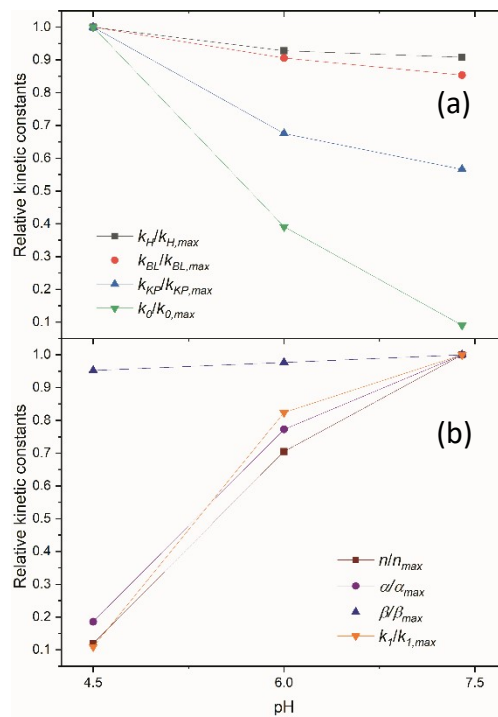


Figure S10. Effect of pH on (a) kinetic constants and (b) exponents values predicting drug release (relative kinetic constants were determined with respect to the highest value obtained).

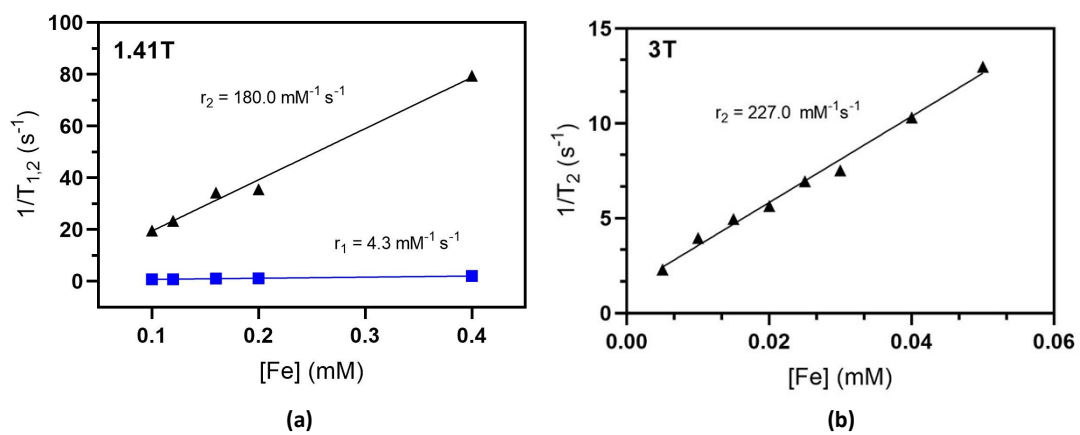


Figure S11. a) Transverse and longitudinal relaxivity (r_1 , r_2) calculation at 1.41T using a Bruker minispec (mq60), b) r_2 calculation at 3T using a MRSolutions preclinical benchtop 3T-MRI scanner.